Electric Power Systems Research 212 (2022) 108567

Contents lists available at ScienceDirect

Electric Power Systems Research

journal homepage: www.elsevier.com/locate/epsr

Optimal grid-forming control of battery energy storage systems providing multiple services: Modeling and experimental validation ☆

Francesco Gerini [a,*], Yihui Zuo [a], Rahul Gupta [a], Antonio Zecchino [a], Zhao Yuan [a], Elena Vagnoni [b], Rachid Cherkaoui [a], Mario Paolone [a]

[a] Distributed Electrical Systems Laboratory (DESL), Ecole Polytechnique Fédérale de Lausanne, EPFL, Lausanne, Switzerland
[b] Technology Platform for Hydraulic Machines (PTMH), Ecole Polytechnique Fédérale de Lausanne, EPFL, Lausanne, Switzerland

ARTICLE INFO

Keywords:
Grid-forming converter
Battery energy storage systems
Frequency containment reserve
Optimal scheduling

ABSTRACT

This paper proposes and experimentally validates a joint control and scheduling framework for a grid-forming converter-interfaced Battery Energy Storage Systems (BESSs) providing multiple services to the electrical grid. The framework is designed to dispatch the operation of a distribution feeder hosting heterogeneous prosumers according to a dispatch plan and to provide frequency containment reserve and voltage control as additional services. The framework consists of three phases. In the day-ahead scheduling phase, a robust optimization problem is solved to compute the optimal dispatch plan and frequency droop coefficient, accounting for the uncertainty of the aggregated prosumption. In the intra-day phase, a model predictive control algorithm is used to compute the power set-point for the BESS to achieve the tracking of the dispatch plan. Finally, in a real-time stage, the power set-point originated by the dispatch tracking is converted into a feasible frequency set-point for the grid forming converter by means of a convex optimization problem accounting for the capability curve of the power converter. The proposed framework is experimentally validated by using a grid-scale 720 kVA/560 kWh BESS connected to a 20 kV distribution feeder in the EPFL campus hosting stochastic prosumption and PV generation.

1. Introduction

1.1. Motivation

Power systems are evolving towards environmentally sustainable networks by increasing the share of renewable power generation interfaced by power converters. The decline of grid inertia levels and a lack of frequency containment delivered by conventional synchronous generators [1,2], in addition to the uncertainty associated to the forecast of renewable resources, require restoring an adequate capability of regulating power to assure reliable operation of interconnected power systems [3].

In this context, network operators are motivated to set strict requirements on the dispatchability of connected resources and to incorporate assets with high ramping capability to maintain frequency containment performance [4,5]. An emerging concept to tackle the challenge of dispatchability of power distribution systems hosting stochastic power generation is to exploit the utility-scale Battery Energy Storage Systems (BESSs). Moreover, in recent years, BESSs are increasingly deployed for ancillary services, thanks to their large ramping capability, high round-trip efficiency, and commercial availability [6,7]. Indeed, the usage of BESSs has been investigated to provide frequency and voltage regulation services [8–13]. In [8], a method for optimal sizing and operation of a BESS used for the frequency containment reserve in a small isolated power system is presented. [9,10] explore the potential use of BESSs participating in frequency regulation markets. [9] proposes an approach that allows LiFePO4 BESSs to achieve the lowest tender price in the *Firm Frequency Regulation* (FFR) market of the UK National Grid. Based on simulations of real *Automatic Generation Control* (AGC) data from a Spanish balancing area, [10] assesses the benefit of utilizing BESSs to improve the dynamic performance of the AGC. In addition, [11] proposes to deploy BESSs to control the voltage of a radial grid characterized by high penetration of distributed

☆ This work is funded in part by the OSMOSE project and in part by the XFLEX HYDRO project. The OSMOSE project has received funding from the European Union's Horizon 2020 research and innovation program under grant agreement No 773406. The XFLEX HYDRO project has received funding from the European Union's Horizon 2020 research and innovation programme under grant agreement No 857832.

* Corresponding author.
E-mail addresses: francesco.gerini@epfl.ch (F. Gerini), yihui.zuo@epfl.ch (Y. Zuo), rahul.gupta@epfl.ch (R. Gupta), antonio.zecchino@epfl.ch (A. Zecchino), zhao.yuan@epfl.ch (Z. Yuan), elena.vagnoni@epfl.ch (E. Vagnoni), rachid.cherkaoui@epfl.ch (R. Cherkaoui), mario.paolone@epfl.ch (M. Paolone).

https://doi.org/10.1016/j.epsr.2022.108567
Received 9 October 2021; Received in revised form 16 April 2022; Accepted 2 July 2022
Available online 25 July 2022

generation and [12] utilizes BESSs to track voltage set-point requested by *Transmission System Operator* (TSO) in an optimal and coordinated manner. Finally, the work in [13] controls a BESS together with other flexible resources to achieve dispatch of a microgrid. Nevertheless, the control strategies proposed in the above studies focus on the provision of a single ancillary service, which may not fully exploit the potential of the BESS. In this respect, control frameworks of BESS providing multiple ancillary services to the power system are of high interest to fully take advantage of BESSs investments [14,15]. The state-of-the-art has presented optimal solution for ancillary services provision [16–18]. In particular, [16] proposes to solve an optimization problem that allocates the battery power and energy budgets to different services in order to maximize battery exploitation. Nevertheless, to the authors' best knowledge, the dispatch tracking problem is oversimplified and does not ensure the BESS operation to be within the physical limits. On the other hand, [17] tackles the problem of dispatching the operation of a cluster of stochastic prosumers through a two-stage process, which consists of a day-ahead dispatch plan determined by the data-driven forecasting and a real-time operation tracking the dispatch plan via adjusting the real power injections of the BESS with a *Model Predictive Control* (MPC). Finally, [18] proposes a control method for BESSs to provide concurrent *Frequency Containment Reserve* (FCR) and local voltage regulation services.

Despite the efforts, all the proposed solutions rely on *grid-following* (GFL) control strategies, therefore ignoring the possibility of controlling the BESS converter in *grid-forming* (GFR) mode. Indeed, BESSs interface with power systems through power converters, which can be controlled as either *grid-forming* or *grid-following* units. For reference, we recall the definitions of GFR and GFL converters from [19]. A GFR converter controls the magnitude and angle of the voltage at its terminals, thus linking the active power exchange with the angle difference between the modulated voltage and the grid voltage at *Point of Common Coupling* (PCC). Therefore, an estimate of grid voltage angle is necessary and can be achieved in two ways: by using a *Phase-Locked Loop* (PLL) or directly linking the active power exchange to the angle difference between the grid and the modulated voltages to create a PLL-free controller. On the other hand, GFL converters control active and reactive power by controlling the amplitude and phase of the injected current with respect to the grid-voltage at the PCC. In this case, a three-phase PLL is required to estimate the fundamental frequency phasor of the grid voltage, so as to generate the instantaneous value of the current reference and, eventually, the voltage reference.

Even if the majority of converter-interfaced resources are currently controlled as grid-following units [20–22], future low-inertia grids are advocated to host a substantiate amount of grid-forming units providing support to both frequency/voltage regulation and system stability [23–25]. Recent studies have proved GFR control strategies to outperform GFL in terms of frequency regulation performance in low-inertia power grids [19]. Furthermore, the impact of GFR converters on the dynamics of a reduced-inertia grids has been investigated in [26], which quantitatively proved the good performance of GFR units in limiting the frequency deviation and in damping the frequency oscillations in case of large power system contingencies. Nevertheless, the existing scientific literature lacks studies assessing the performance of GFR units in supporting the frequency containment process of large interconnected power grids. Moreover, to the best of the authors knowledge, GFR units have never been proved able to provide services such as feeder dispatchability. In fact, studies on the GFR units synchronizing with AC grids are mostly limited to ancillary services provision and their validations is based on either simulation [19]–[27] or experiments on ideal slack buses with emulated voltage [28,29].

1.2. Paper's contribution

With respect to the existing literature discussed in the previous section, the contributions of this paper are the following.

- The development of a control framework for GFR converter-interfaced BESS, tackling the optimal provision of multiple services, which relies on existing grid-following control strategies [16–18]. The control framework for the simultaneous provision of feeder dispatchability, FCR and voltage regulation aims to maximize the battery exploitation in the presence of uncertainties due to stochastic demand, distributed generation, and grid frequency.
- The experimental validation of the proposed framework by using a 560 kWh BESS interfaced with a 720 kVA GFR-controlled converter to dispatch the operation of a 20 kV distribution feeder hosting both conventional consumption and distributed *Photo-Voltaic* (PV) generation.
- The performance assessment of the GFR-controlled BESS providing simultaneously dispatching tracking and FCR provision. In particular, the frequency regulation performance of the GFR-controlled BESS is evaluated and compared with the case of GFR only providing FCR and with the GFL case.

The paper is organized as follows. Section 2 proposes the general formulation of the control problem for the BESS providing multiple services simultaneously. Section 3 presents a detailed description of the three-stage control framework. Section 4 provides the validation of the proposed framework by means of real-scale experiments. Finally, Section 5 summarizes the original contributions and main outcomes of the paper and proposes perspectives for further research activities.

2. Problem statement

2.1. Outline of the control framework for grid-forming BESSs

In this paper, the dispatchability of distribution feeders and the simultaneous provision of FCR and voltage regulation is tackled by controlling a grid-forming converter-interfaced BESS. Specifically, the framework ensures the control of the operation of a group of prosumers (characterized by both conventional demand and PV generation that are assumed to be uncontrollable) according to a scheduled power trajectory at 5 min resolution, called dispatch plan, determined the day before operation. The day-ahead scheduler relies on a forecast of the local prosumption. The multiple-service-oriented framework consists of three stages as summarized by Fig. 1 where each stage is characterized by a different time horizon:

(i) The dispatch plan is computed on the day-ahead (i.e., in agreement with most common practices), where the feeder operator determines a dispatch plan based on the forecast of the prosumption while accounting also for the regulation capacity of BESSs [30]. Specifically, an optimization problem is solved to allocate the battery power and energy budgets to the different services by determining a dispatch plan at a 5-minute resolution based on the forecast of the prosumption and computing the droop for the FCR provision.

(ii) In the intermediate level stage, with a 5-minute horizon, the active power injections of the BESS are adjusted by means of a MPC, targeting both the correction of the mismatch between prosumption and dispatch plan (as proposed by [17]) and the FCR provision. The MPC is actuated every 10 s to both ensure a correct tracking over the 5 min window and avoid overlapping the dispatch tracking with the FCR action.

(iii) In the final stage, computed each second, the MPC active power command is converted into a feasible frequency set-point for the GFR converter. As a matter of fact, the feasible PQ region of the BESS power converter is a function of the battery DC-link and AC-grid status [18]. For this reason, the feasibility of the grid-forming frequency reference set-point is ensured by solving every second an efficient optimization problem that takes into account the dynamic capability curve of the DC–AC converter and adjusts the set point accordingly. Eventually, the

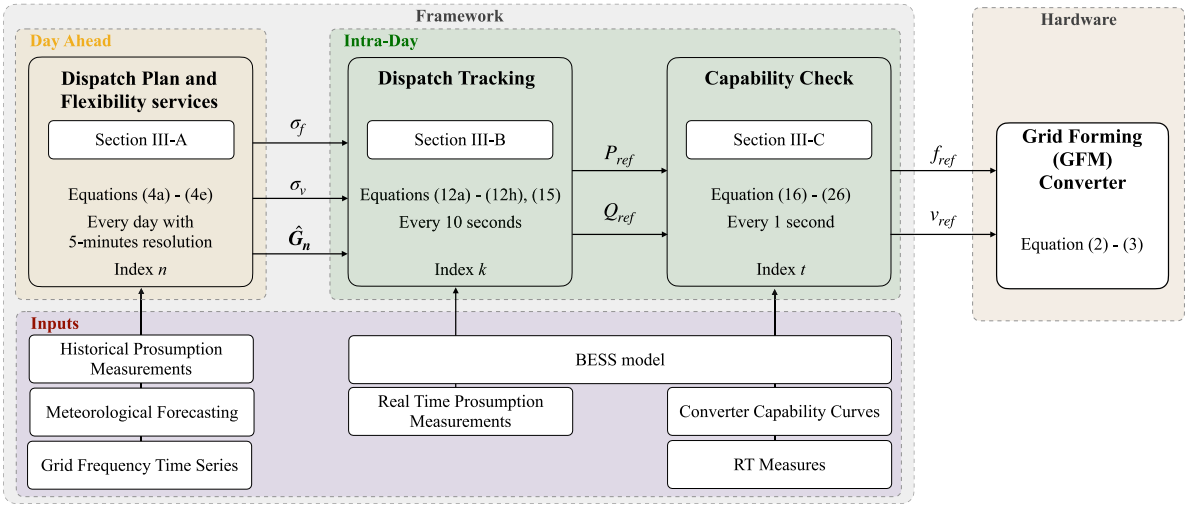

Fig. 1. Outline of the control framework for grid-forming BESSs.

feasible frequency set-point is implemented in the GFR controller which intrinsically superposes the frequency control action on the active power dispatch.

2.2. Regulatory framework

Since the framework is developed with the purpose of enhancing the provision of different ancillary services, it is necessary to consider the corresponding regulatory framework. As the experimental activities are performed at the EPFL campus, in Lausanne (Switzerland), the paper refers to the grid code of the Swiss TSO, SwissGrid [31–35]. Nevertheless, the rules for other European TSOs are mostly similar. The most important aspects are the tender periods for the ancillary services market and the technical requirements to be considered eligible to provide a specific service.

2.2.1. Tender period

The choice of the timing for the droop computation is related to the market regulating the provision of ancillary services. Different balancing and ancillary services markets in EU member states have different market closing times for the procurement of the ancillary services, as well as different sets of participants and activation time [36]. Therefore, the choice of the time horizon for the droop computation is market/country-dependent. By referring to [32], the SwissGrid calls for the tender of FCR provision every day, i.e., one day ahead with respect to the delivery date. Moreover, a platform operated on a daily basis has been established in Germany for sharing the reserves among the TSOs from Germany, France, Belgium, the Netherlands, Austria and Switzerland [37]. These are the reasons that justify the authors' choice of computing the droop with intervals of one day.

2.2.2. Technical requirement

The technical requirements fixed by TSOs on the insensitivity range[1] and activation speed [33] can be easily fulfilled by BESSs, as the requests are rather mild when compared with the BESSs' large ramping capability [39,40]. The most constraining requirement for BESS is the necessity of ensuring continuous activation [34] for at least 15 min for a deviation of 200 mHz in the grid frequency. This constraint is implemented in the day-ahead section of the proposed framework in terms of limits on the values of State-of-Energy of the BESS, i.e., SOE_{min} and SOE_{max}.

[1] Frequency dead-band under which no FCR action is required, typically around 10 mHz in the ENTSO continental Europe synchronous area [38].

2.2.3. Provision of multiple service

According to [35], when a dispatch plan is defined with the TSO, any additional service provided must consider the dispatch plan as a basis for the evaluation of the service. That is, if dispatchability and FCR are simultaneously provided, the dispatch plan represents the base for the evaluation of the FCR service. To comply with this request, the term ΔG_k^F, defined in Eq. (11) is added to Eq. (10).

3. Control framework

3.1. Day-ahead stage

The objective of the day ahead is to compute a dispatch plan $\hat{\boldsymbol{G}}$ for a distribution feeder and to simultaneously contract with the TSO a certain frequency droop for the BESS FCR provision. A representation of the feeder and the corresponding power flows is shown in Fig. 2. The BESS bidirectional real power flow is denoted by P, while G is the composite power flow as seen at the *Point of Common Coupling* (PCC). The aggregated building demand is denoted by L and, if grid losses are neglected, it is estimated as:

$$L = G - P \tag{1}$$

On top of achieving feeder dispatchability, the proposed framework allows the GFR-controlled BESS to react to the grid-frequency variation in real time, i.e., providing FCR. The latter action is automatically performed by the converter operated in GFR mode, where the power flowing through the BESS can be computed as:

$$P = \sigma_f \cdot (f - f_{ref}) \tag{2}$$

$$Q = \sigma_v \cdot (v - v_{ref}) \tag{3}$$

In Eqs. (2) and (3) σ_f and σ_v are respectively the frequency and voltage droop[2] fixed at the day-ahead stage, while f_{ref} and v_{ref} are the frequency and voltage reference set-point (i.e., real-time command) of the GFR converter. The target of the control problem is to regulate the composite power flow G to respect the dispatch plan fixed on the day-ahead planning and the frequency containment action accorded with the TSO.

[2] While the σ_f is computed in the day-ahead problem for the FCR service, the σ_v is considered to allow for adjusting reactive power in the real-time stage (see in Section 3.3) and is determined according to the voltage control practice recommend in [38].

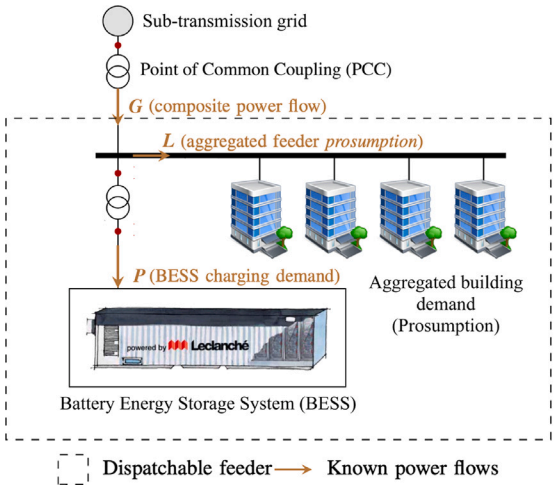

Fig. 2. General feeder configuration used for the problem statement. The distribution feeder includes a group of buildings hosting stochastic and uncontrollable PV installations and a grid-connected BESS. The grid has a radial topology. The BESS is the sole controllable resource of the feeder. Dispatch and grid services are considered to be provided at the PCC.

The formulation of the day-ahead problem considering the provision of both FCR and dispatchability proposed by [16] can be adapted to the grid-forming case. The mathematical formulation is hereby proposed:

$$[\sigma_f^0, \boldsymbol{F}^o] = \underset{\sigma_f \in \mathbb{R}^+, \boldsymbol{F} \in \mathbb{R}^N}{\arg\max} \ (\sigma_f) \tag{4a}$$

subject to:

$$SOE_0 + \frac{1}{E_{\text{nom}}}\left[\frac{T}{N}\sum_{i=0}^{n}(F_i + L_i^{\uparrow}) + \sigma_f W_{f,n}^{\uparrow}\right] \leq SOE_{\max}, \tag{4b}$$

$$SOE_0 + \frac{1}{E_{\text{nom}}}\left[\frac{T}{N}\sum_{i=0}^{n}(F_i + L_i^{\downarrow}) + \sigma_f W_{f,n}^{\downarrow}\right] \geq SOE_{\min}, \tag{4c}$$

$$F_n + L_n^{\uparrow} + 0.2\sigma_f \geq P_{\max}, \tag{4d}$$

$$F_n + L_n^{\downarrow} + 0.2\sigma_f \leq P_{\max}, \tag{4e}$$

where:

- T is the total scheduling time window (i.e., $T = 86400$ s) discretized in N time steps ($N = 288$, i.e., the dispatch plan is divided into 5 min windows) and each step is denoted by the subscript n with $n = 0, \dots, N-1$.
- $\hat{\boldsymbol{L}} = \hat{L}_1, \dots, \hat{L}_N$ is the forecast profile of feeder prosumption and $\boldsymbol{F^o} = F_1, \dots, F_N$ is the BESS power offset profile which is computed to keep the BESS stored energy at a value capable of compensating for the difference between prosumers' forecasted and realized power. The day-ahead dispatch plan $\hat{\boldsymbol{G}} = \hat{G}_1, \dots, \hat{G}_N$ is the sum of the above two terms, as in Eq. (1).
- σ_f is the FCR droop expressed in kW/Hz
- $W_{f,k}$ denotes the integral of frequency deviations over a period of time, and it represents the energy content of the signal given by the frequency deviation from its nominal value.
- The BESS limits in terms of *State Of Energy* (SOE) and power are expressed respectively with $SOE_{\min}$, $SOE_{\max}$, $P_{\min}$ and $P_{\max}$, while E_{nom} is the nominal BESS energy.

It is worth mentioning that the optimization problem described by Eqs. (4a)–(4e) prioritizes the dispatchability of the feeder over the FCR provision on the day-ahead planning. This choice is nevertheless user-dependent, based on the economical convenience of the provided service or on grid core requirements. For example, if the user stipulates a contract with the TSO for FCR provision, this service can be prioritized, and the remaining energy can be allocated for the dispatch service, which will, inevitably, not always be achieved if the prosumption stochasticity is too high.[3]

3.2. Intra-day stage

In the intra-day stage a MPC algorithm is used to target the fulfillment of the mismatch between average prosumption for each 5-minute period and the combined dispatch plan and FCR action agreed upon with the TSO for the same time-window. Since the MPC action has a time-sampling of 10 s, the index $k = 0, 1, 2, \dots, K-1$ is introduced to denote the rolling 10 s time interval, where $K = 8640$ is the number of 10 s periods in 24 h. The value of the prosumption set-point retrieved from the dispatch plan for the current 5-minute slot is indicated by the k-index as:

$$G_k^* = \hat{G}_{\lfloor \frac{k}{30} \rfloor} \tag{5}$$

where $\lfloor \cdot \rfloor$ denotes the nearest lower integer of the argument, and 30 is the number of 10-second interval in a 5-minute slot. The first and the last 10-second interval for the current 5-minutes are denoted as $\underline{k}$ and $\overline{k}$, respectively:

$$\underline{k} = \lfloor \frac{k}{30} \rfloor \cdot 30 \tag{6}$$

$$\overline{k} = \underline{k} + 30 - 1 \tag{7}$$

A graphical representation of the execution timeline for the MPC problem is given by Fig. 3 displaying the first thirty-one 10-seconds intervals of the day of operation. The figure shows the BESS power set-point $P_2{}^\circ$, which has been computed by knowing the prosumption realizations L_0 and L_1, and the average prosumption set-point to be achieved in the 5-minute interval (i.e., first value of the dispatch plan $\hat{G}_0$). A similar control problem, not including the simultaneous provision of FCR by the BESS, is described in [17]. For this reason, the MPC problem proposed in [17] is modified as follows, to account for the provision of multiple services by means of GFR converter. Considering Eq. (1), the average composite power flow at the PCC (prosumption + BESS injection) is given by averaging the available information until k as:

$$G_k = \frac{1}{k - \underline{k}} \cdot \sum_{j=\underline{k}}^{k-1}(L_j + P_j) \tag{8}$$

Then, it is possible to compute the expected average composite flow at the PCC at the end of the 5 min window as:

$$G_k^+ = \frac{1}{30}\left((k - \underline{k}) \cdot G_k + \sum_{j=k}^{\overline{k}} \hat{L}_{j|k}\right) \tag{9}$$

where a persistent,[4] forecast is used to model future realizations, namely $\hat{L}_{j|k} = L_{k-1}, j = k, \dots, \overline{k}$. The energy error between the realization and the target (i.e. dispatch plan plus FCR energy) in the 5-minute slot is expressed (in kWh) as:

$$e_k = \frac{300}{3600} \cdot (G_k^* - G_k^+ + \Delta G_k^F) \tag{10}$$

where 300 s and 3600 s are the number of seconds in a 5 min interval and 1 h interval, respectively. The additional term ΔG_k^F considers the deviation caused by the frequency containment response of the GFR converter:

$$\Delta G_k^F = \frac{1}{30}\sum_{j=\underline{k}}^{k-1}(50 - f_j) \cdot \sigma_f \tag{11}$$

[3] Further discussion can be found in Section 4.

[4] As shown in [41] the persistent predictor performs well given the short MPC horizon time and fast control actuation in this application.

where f_j is the frequency measurement at time j. Finally, the MPC can be formulated to minimize the error e_k over the 5-minutes window, subject to a set of physical constraints such as BESS SOC, DC voltage and current operational limit. It should be noted that including the term ΔG_k^F in the energy error function fed to the MPC allows for decoupling the dispatch plan tracking with the frequency containment response provided by the BESS in each 5-minute slot. In particular, the omission of this term while operating the BESS in GFR mode, can create conflicts between dispatch plan tracking and frequency containment provision. As in [17], in order to achieve a convex formulation of the optimization problem, the proposed MPC problem targets the maximization of the sum of the equally weighted BESS DC-side current values over the shrinking horizon from k to $\bar{k}$ in its objective (12a) while constraining the total energy throughput to be smaller or equal to the target energy e_k. The optimization problem is formulated as:

$$\boldsymbol{i}^o_{\bar{k}|k} = \underset{i\in\mathbb{R}^{(k-\bar{k}+1)}}{\arg\max}(\mathbf{1}^T \boldsymbol{i}_{\bar{k}|k}) \tag{12a}$$

subject to:

$$\alpha \boldsymbol{v}^T_{\bar{k}|k} \boldsymbol{i}_{\bar{k}|k} \preceq e_k \tag{12b}$$

$$\mathbf{1}\cdot i_{min} \preceq \boldsymbol{i}_{\bar{k}|k} \preceq \mathbf{1}\cdot i_{max} \tag{12c}$$

$$\mathbf{1}\cdot \Delta i_{min} \preceq H\boldsymbol{i}_{\bar{k}|k} \preceq \mathbf{1}\cdot \Delta i_{max} \tag{12d}$$

$$\boldsymbol{v}_{\bar{k}|k} = \phi_v x_k + \psi^v_i \boldsymbol{i}_{\bar{k}|k} + \psi^v_1 \mathbf{1} \tag{12e}$$

$$\mathbf{1}\cdot v_{min} \preceq \boldsymbol{v}_{\bar{k}|k} \preceq \mathbf{1}\cdot v_{max} \tag{12f}$$

$$\mathbf{SOC}_{\bar{k}|k} = \phi^{\mathrm{SOC}}\mathrm{SOC}_k + \psi^{\mathrm{SOC}}_i i_{\bar{k}|k} \tag{12g}$$

$$\mathbf{1}\cdot \mathrm{SOC}_{min} \preceq \mathbf{SOC}_{\bar{k}|k} \preceq \mathbf{1}\cdot \mathrm{SOC}_{max} \tag{12h}$$

where

- $\boldsymbol{i}^o_{\bar{k}|k}$ is the computed control action trajectory, $\mathbf{1}$ denotes the all-ones column vector, the symbol $\preceq$ is the component-wise inequality, and the bold notation denotes the sequences obtained by stacking in column vectors the realizations in time of the referenced variables, e.g. $\boldsymbol{v}_{\bar{k}|k} = [v_k, \dots, v_{\bar{k}}]^T$.
- In (12b), the BESS energy throughput (in kWh) on the AC bus is modeled as $E_{\bar{k}|k}(\cdot) = \alpha \boldsymbol{v}^T_{\bar{k}|k} \boldsymbol{i}_{\bar{k}|k}$, where $\boldsymbol{v}_{\bar{k}|k}$ and $\boldsymbol{i}_{\bar{k}|k}$ are the battery DC voltage and current, respectively, and $\alpha = 10/3600$ is a converting factor from average power over 10 s to energy expressed in kWh.
- The inequality (12c) and (12d) are the constraints on the magnitude and rate of change for the BESS current, respectively. The matrix $H \in \mathbb{R}^{(k-\bar{k}+1)\times(k-\bar{k}+1)}$ is

$$H = \begin{bmatrix} 1 & -1 & 0 & 0 & \dots & 0 \\ 0 & 1 & -1 & 0 & \dots & 0 \\ \vdots & \vdots & \vdots & \vdots & \vdots & \vdots \\ 0 & 0 & 0 & \dots & 1 & -1 \end{bmatrix} \tag{13}$$

- The equality (12e) is the *Three-Time-Constant (TTC)* electrical equivalent circuit model of the voltage on DC bus, whose dynamic evolution can be expressed as a linear function of battery current by applying the transition matrices ϕ^v, ψ^v, ψ^v_1. x_k is the state vector of the voltage model.[5] The inequality (12f) defines the BESS voltage limits. The TTC model for computing the DC voltage and the estimation of x_k are described in [17].

[5] This modeling choice is taken according to [17], where a more accurate model, compared with the commonly adopted two-time constant model in the literature [42], is implemented. The TTC model allows to better capture dynamics of BESSs, in case the future development of the framework will require the MPC problem to be solved with smaller time step. Nevertheless, to compute the BESS predictions with a 10 s time horizon, lower order models could be used.

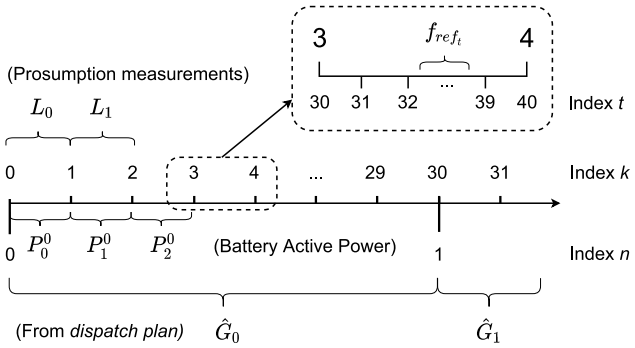

Fig. 3. Timeline of the control framework. The dispatch plan and the allocation of ancillary services are computed on the day ahead. The dispatch plan $\hat{G}$ has a time resolution of 5 min (discrete time index n). During the day, the MPC problem is executed every 10 s (discrete time index k). Finally, the RT problem computes the final f_{ref}, v_{ref} set-points every second t.

- The equality (12g) is the evolution of the BESS SOC as linear function of the variable $\boldsymbol{i}^o_{\bar{k}|k}$, where ϕ^{SOC} and ψ^{SOC}_i are transient matrices obtained from the BESS SOC model:

$$SOC_{k+1} = SOC_k + \frac{10}{3600}\frac{i_k}{C_{nom}} \tag{14}$$

  where C_{nom} is BESS capacity in [Ah]. The discritized state-space matrix for the SOC model can be easily obtained from (14) with $A_s = 1$, $B_s = 10/3600/C_{nom}$, $C_s = 1$, $D_s = 0$. Finally, (12h) enforces the limits on BESS SOC.

The optimization problem is solved at each time step k obtaining the control trajectory for the whole residual horizon from the index k to $\bar{k}$, i.e., $\boldsymbol{i}_{\bar{k}|k}$. However, only the first component of the current control trajectory is considered for actuation, i.e., $\boldsymbol{i}^o_{\bar{k}|k}$. Finally, $\boldsymbol{i}^o_{\bar{k}|k}$ is transformed into a power set-point P^0_k, computed as:

$$P^0_k = v_k \cdot i^o_k \tag{15}$$

3.3. Real-time control stage

The real-time control stage is the final stage of the framework, whose output f_{ref}, v_{ref} is the input for the GFR BESS converter. Thanks to the day-ahead problem, sufficient BESS energy capacity is guaranteed in the MPC tracking problem. To ensure the BESS operation to be within the power limits, a static physical constraint of control actions is considered in the day-ahead stage in (4d) and (4e) and during the dispatch tracking in (12c) and (12d). Nevertheless, these constraints do not account for the dependency of the converter feasible PQ region on DC voltage and AC grid voltage conditions since they are only known in real time. In this respect, the real-time controller is implemented to both keep the converter operating in the PQ feasible region identified by the capability curve and to convert the power set-point from the MPC problem into a frequency reference set-point to feed the GFR converter.

3.3.1. Capability curve

As proved in [18], the converter PQ capability curve h can be modeled as a function of the BESS DC voltage v^{DC}_t and the module of the direct sequence component of the phase-to-phase BESS AC side voltages v^{AC}_t at time $t \in [1, 2, \dots, T]$ as:

$$h(P_t, Q_t, v^{DC}_t, v^{AC}_t, SOC_t) \le 0 \tag{16}$$

where the BESS SOC is considered for the selection of the capability curve because the estimation of v^{DC}_t relies on the battery TTC model whose parameters are SOC-dependent [18]. In particular, the v^{DC}_t is

estimated using the TTC model of DC voltage, thus, the same formula as (12e):

$$v_t^{DC} = \phi_v x_t + \psi_i^v i_t^{DC} + \psi_1^v \mathbf{1} \tag{17}$$

Eq. (17) is solved together with the charging or discharging DC current equation as follows:

$$i_t^{DC} \approx \frac{P_t^{DC}}{v_t^{DC}} \tag{18}$$

where the active power at the DC bus is related to the active power set-point AC side of the converter as:

$$P_t^{DC} = \begin{cases} \eta P_{set,t}, & \forall P_{set,t} < 0 \\ P_{set,t}/\eta, & \forall P_{set,t} \leq 0 \end{cases} \tag{19}$$

where η is the efficiency of converter, $P_{set,t}$ is the set-point from the MPC, computed in (15) and expressed as:

$$P_{set,t} = P^0_{\lfloor \frac{t}{10} \rfloor} \tag{20}$$

Once the DC voltage v_t^{DC} is known, the magnitude of the direct sequence component v_t^{AC} of the phase-to-phase voltage at AC side of the converter is estimated via the Thévenin equivalent circuit of the AC grid, expressed as

$$v_t^{AC} \approx \sqrt{(v_t^{AC,m})^2 + X_T^2 \frac{(P_{set,t})^2 + (Q_{set,t})^2}{3(v_t^{AC,m})^2}} \tag{21}$$

where the primary side voltage $v_t^{AC,MV}$ is referred to the secondary side as $v_t^{AC,m} = v_t^{AC,MV} \frac{1}{n}$, being n the transformer ratio, $v_t^{AC,MV}$ is the voltage measured at the primary side of the transformer, and X_T is the reactance of the step-up transformer, as shown in Fig. 2. Eqs. (16) to (21) represent the relation between active and reactive power set-points with the converter capability curve.

3.3.2. Set-point conversion for GFR converters

Together with a feasibility check for the power set-point $P_{set,t}$, the real time controller is responsible for converting the power set-point into a frequency reference set-point to feed the GFR converter. In particular, the power output of a GFR converter can be expressed, starting from Eq. (22), as:

$$P = \sigma_f \cdot (f - f_{\text{nom}}) + \sigma_f \cdot (f_{\text{nom}} - f_{ref,t}) = P_{fcr} + P_{set,t} \tag{22}$$

where f_{nom} is the nominal frequency, the term P_{fcr} corresponds to the power delivered with respect to the frequency containment action, f is the grid frequency.[6] As visible from Eq. (22), the relation between the power set-point P_{set} of the GFR converter and the input f_{ref} is linear:

$$P_{set,t} = \sigma_f \cdot (f_{\text{nom}} - f_{ref,t}) \tag{23}$$

Similarly, for the reactive power:

$$Q_{set,t} = \sigma_v \cdot (v_{\text{nom}} - v_{ref,t}) \tag{24}$$

where v_{nom} is the nominal voltage. Eqs. (23) to (24) represent the relation between active/reactive power and frequency/voltage set-point fed to a GFR converter.

[6] It should be noted that the frequency control action P_{fcr} and the grid frequency f are not denoted with subscript t because they are not controlled variables in the optimization problem. Instead, f depends on the interconnected power grid and P_{fcr} is the automatic response of GFR control with response time in the order of tens of milliseconds.

3.3.3. Real-time problem formulation

Finally, given a set-point in power $P_{set,t}, Q_{set,t}$ (in order to prioritize the active power, the reactive power set-point $Q_{set,t}$ can be set as zero) coming from the MPC problem, the GFR converter optimal references are computed by solving the following optimization problem:

$$\begin{aligned} &[f^*_{ref,t}, v^*_{ref,t}] = \\ &= \arg\min \lambda_P (P^*_{set} - P_{set,t})^2 + \lambda_Q (Q^*_{set} - Q_{set,t})^2 \end{aligned} \tag{25}$$

subject to (16)–(24), where (16)–(21) represent the relation between active/reactive power with the converter capability curve and (23), (24) represent the relation between active/reactive power with frequency/voltage set-point fed to the GFR controller. A way to convexify the problem in (25) subject to (16)–(21) has been presented in [18], while constraints (23) - (24) are linear, since σ_f and σ_v are fixed. The optimization problem is defined to find the optimal active and reactive power set-point compatibly with the capability curve of the converter. In particular, if the original set-points are feasible, the optimization problem returns the obvious solution $P^*_{set} = P_{set,t}$ and the converter reference points are:

$$f^*_{ref} = f_{\text{nom}} - \frac{P^*_{set}}{\sigma_f} \tag{26}$$

$$v^*_{ref} = v_{\text{nom}} - \frac{Q^*_{set}}{\sigma_v} \tag{27}$$

4. Results

4.1. Experimental setup

For the experimental campaign, a 20 kV distribution feeder in the EPFL campus equipped with a BESS is considered, as shown in Fig. 2. The distribution feeder includes a group of buildings characterized by a 140 kW base load, hosting 105 kWp root-top PV installation and a grid-connected 720 kVA/500 kWh Lithium Titanate BESS.

The BESS is interfaced with the grid through a three-phase, two-level converter with IGBT/Diodes pairs and characterized by: (i) a rated Power of 720 kVA (ii) a nominal AC voltage of 300 V (iii) a DC voltage ranging from 500 to 890 V (iv) a rated DC Current of 1360 A (v) and a round-trip efficiency ≥ 97% The targeted grid has a radial topology and is characterized by co-axial cables lines with a cross section of 95 mm^2 and a length of few hundreds meters, therefore, the grid losses are negligible [43]. The measuring systems is composed by a Phasor Measurement Unit (PMU)-based distributed sensing infrastructure. The measuring infrastructure allows for acquiring in real time accurate information of the power flows G, L and P, thanks to the PMUs' fast reporting rate (i.e., 50 frame per second) and high accuracy which in terms of 1 standard deviation is equal to 0.001 degrees (i.e. 18 μrad) [44].

4.2. Experimental validation

This subsection reports the results of a day-long experiment, taking place on the EPFL campus on a working day (Friday, i.e., day-category C according to Appendix).

4.2.1. Day ahead

The input and output information of the day-ahead dispatch process for the experimental day are shown in Fig. 4. The $S = 10$ generated scenarios $\boldsymbol{C}$ for the prosumption are shown in Fig. 4(a), where $\boldsymbol{C}^{\downarrow}$ and $\boldsymbol{C}^{\uparrow}$ are the lower and upper bounds shown in thick black lines, while all the scenarios are represented by thin colored lines. The upper and lower bound of the PV forecast, expressed in terms of PV production in kW, are shown in Fig. 4(b), while the net demand scenarios at the PCC, obtained according to Eqs. (31) and (32), are shown in Fig. 4(c). The upper and lower bound of the prosumption, namely $L_n^{\uparrow}$ and $L_n^{\downarrow}$, are inputs to the dispatch plan. Finally, Figs. 4(d) and 4(e) show

Table 1
Tracking error statistics (in kW).

	ME	MAE	RMSE
No dispatch tracking	−3.49	47.00	18.26
Dispatch tracking	0.11	16.93	3.00
Dispatch + FCR tracking	−0.45	0.79	1.43

respectively the power and energy budget allocated for the forecasting uncertainty of the stochastic PV production (in dark gray) and demand (in light gray). The remaining energy budget is allocated for the FCR service, resulting in a droop $\sigma_f = 116$ kW/Hz.

4.2.2. Dispatch tracking

The results of the dispatch tracking are visible in Fig. 5. In particular, Fig. 5(a) shows the power at the PCC (in shaded gray), the prosumption (in dashed red) and the dispatch plan (in black). It is observed that the dispatch plan is tracked by the GFR-converter-interfaced BESS when the grid-frequency (visible in Fig. 5(b)) is close to 50 Hz. Nonetheless, when the grid-frequency has a significant deviation from 50 Hz, the GFR converter provides a non-negligible amount of power ΔG^F to the feeder. This contribution is visible in shaded blue in Fig. 5(a), and causes a deviation of the average PCC power from the dispatch plan, as targeted by Eq. (9). Moreover, as visible in Fig. 5(c) the BESS SOE is contained within its physical limits over the day. To evaluate the dispatch plan-tracking performance, *Root Mean Square Error* (RMSE), *Mean Error* (ME), and *Maximum Absolute Error* (MAE) are considered. In particular these indicators are visible in Table 1 for three different cases: (i) no dispatch tracking case, where the error is computed as difference between prosumption and dispatch plan; (ii) dispatch tracking case, where the error is computed as difference between flow at the PCC and dispatch plan; (iii) dispatch tracking + FCR case, where the error is computed as difference between flow at the PCC and dispatch plan + FCR contribution, as targeted by the MPC problem (12a). The obtained results demonstrate the good performance of the dispatch + FCR tracking framework. The overall results are comparable with the one presented in [17]. ì, even though the tracking problem in this study is complicated by the fact that the BESS is operated with a grid-forming converter providing frequency regulation.

4.2.3. Frequency regulation

To assess the performance of the GFR converter in regulating the frequency at the PCC, we adopt the metric relative Rate-of-Change-of-Frequency (rRoCoF) proposed in [45], defined as:

$$rRoCoF = \left| \frac{\Delta f_{PCC}/\Delta t}{\Delta P} \right| \tag{28}$$

where Δf_{PCC} is the difference between one grid-frequency sample and the next (once-differentiated value) at the PCC, ΔP is the once-differentiated BESS active power, and Δt is the sampling interval. As the metric rRoCoF is weighted by the delivered active power of the BESS, it can also be used to compare the effectiveness of converter controls (i.e., GFR vs GFL) in regulating frequency at local level in a large interconnected power system. The grid-frequency is measured by a PMU installed at the PCC.

The rRoCoF is computed from different frequency timeseries, corresponding to the following four cases.

- *Case 1*: rRoCoF computed considering the 24 hour-long experiment where GFR-controlled BESS is providing multiple services.
- *Case 2*: rRoCoF computed considering a 15 min window around a significant frequency transient (i.e., around 00:00 CET) during the same day-long experiment.
- *Case 3*: rRoCoF computed with a dedicated 15 min experiment where GFR-controlled BESS is only providing FCR with its highest possible frequency-droop (1440 kW/Hz) during a significant grid-frequency transient.

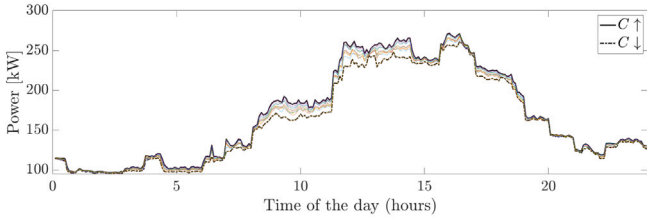

(a) Day-ahead load scenarios

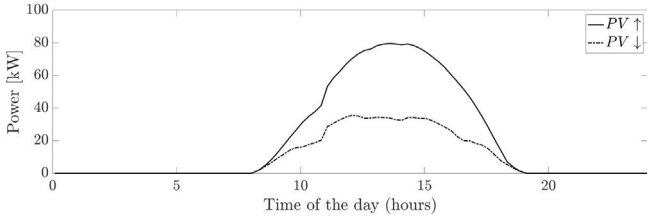

(b) Day-ahead PV forecast

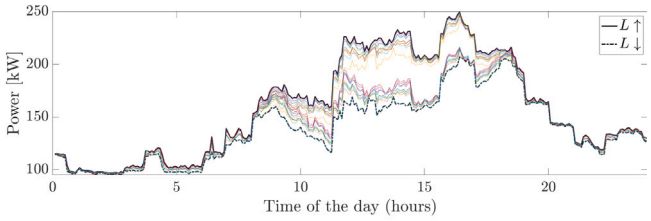

(c) Day-ahead net demand scenarios

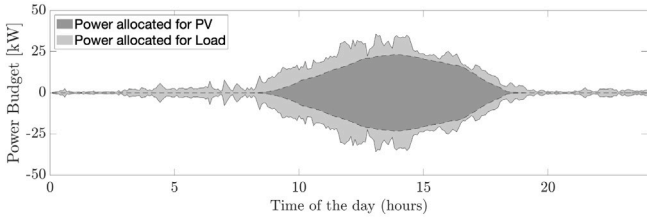

(d) BESS power budget

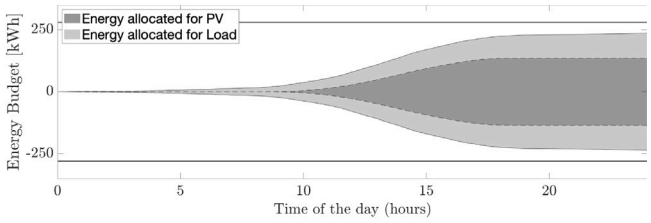

(e) BESS energy budget

Fig. 4. Input and output of the day-ahead problem. (a) shows 10 demand generated scenarios, and their relative upper and lower bound. (b) shows the upper and lower bound for the PV production. (c) combines load and PV to show the prosumption scenario, input of the day ahead problem. (d) and (e) show the power and energy budget allocated to perform the different services.

- *Case 4*: rRoCoF computed with a dedicated 15 min experiment where GFL-controlled BESS is only providing FCR with its highest possible frequency-droop (1440 kW/Hz) during a significant grid-frequency transient.

While *Case 1* and *Case 2* rely on the measurements obtained from the experiment carried out in this study, *Case 3* and *Case 4* leverage an historical frequency data-set, also used in the experimental validation proposed in [45]. It should be noted that the same experimental setup described in Section 4.1 is utilized in [45]. The measurements at hour

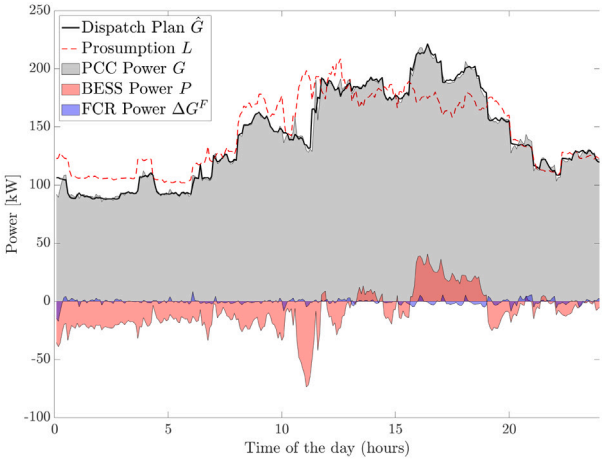

(a) Day-ahead load scenarios

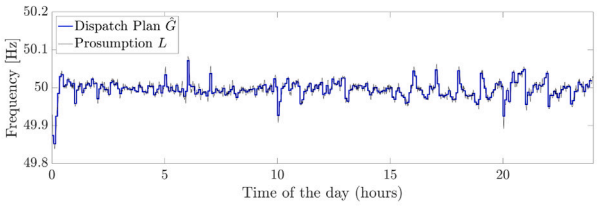

(b) Day-ahead PV forecast

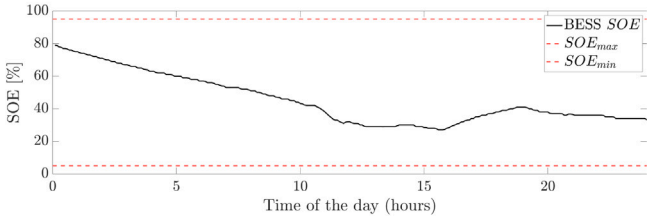

(c) Day-ahead net demand scenarios

Fig. 5. Experimental results for the 24 h test. (a) compares the dispatch plan (in black) with: the measured power at the PCC (shaded gray), the prosumption of the feeder (in dashed red), the BESS power flow (in shaded red) and the average power required for each 5 min window for the provision of FCR service by the BESS. (b) shows the grid-frequency and its 5 min mean. The SOE of the battery during the test is visible in (c).

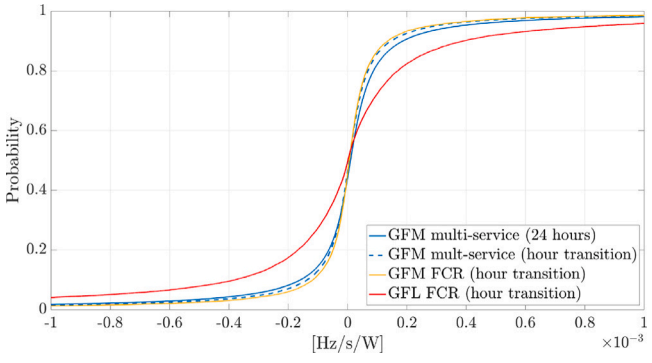

Fig. 6. Cumulative Density Function of rRoCoF.

transition are considered in order to evaluate GFR/GFL units' frequency regulation performance under relatively large frequency variations.

Fig. 6 shows the *Cumulative Density Function* (CDF) of the rRoCoF values for the four cases. First, it is observed that the CDF results of *Case 1* and *Case 2* are very close. This illustrates the robustness of the metric rRoCoF. In particular since rRoCoF is normalized by the BESS power injection, the frequency dynamic and the frequency droop of the BESS controller have little effect on the result of CDF. Moreover, the comparison between *Case 2* and *Case 3* shows negligible differences on the rRoCoF CDF, proving that the provision of dispatchability service by the GFR converter does not drastically affect its frequency regulation performance. Finally, the comparison between GFR and GFL-controlled BESS (i.e., *Case 2* vs *Case 4*) is reported from [45], to show that GFR unit achieves significantly lower rRoCoF for per watt of regulating power injected by the BESS.

5. Conclusions

A comprehensive framework for the simultaneous provision of multiple services (i.e., feeder dispatchability, frequency and voltage regulation) to the grid by means of a GFR-converter-interfaced BESS has been proposed. The framework consists of three stages. The day-ahead stage determines an optimal dispatch plan and a maximum frequency droop coefficient by solving a robust optimization problem that accounts for the uncertainty of forecasted prosumption. In the intra-day stage, a MPC method is used in the operation process to achieve the tracking of dispatch plan while allowing for frequency containment reserve properly delivered by the BESS. Finally, the real-time controller is implemented to convert the power set-points from MPC into frequency references accounting for the PQ feasible region of the converter.

The experimental campaign is carried out in a 20 kV distribution feeder in the EPFL campus. The feeder includes a group of buildings characterized by a 140 kW base load, hosting 105 kWp root-top PV installation and a grid-connected 720 kVA/500 kWh Lithium Titanate BESS. A 24 h long experiment demonstrated good performance in terms of dispatch tracking, comparable with the results obtained in [17] for sole provision of dispatchability by means of GFL converter-interfaced BESS. Moreover, the rRoCoF metric has been used to shows that the provision of dispatchability service by the GFR converter does not affect its frequency regulation performance and confirm the positive effects of grid-forming converters with respect to the grid-following ones in the control of the local frequency. Future works concern the development of control strategies to prioritize the FCR service when the battery is operating close to its operational limit, as required by grid-codes. Moreover, an analysis on the effects of voltage regulation on the BESS losses could be included in the day ahead scheduling problem.

CRediT authorship contribution statement

Francesco Gerini: Conceptualization, Methodology, Writing – original draft, Software. **Yihui Zuo:** Conceptualization, Methodology, Writing – original draft, Software. **Rahul Gupta:** Conceptualization, Methodology, Writing – original draft, Software. **Antonio Zecchino:** Data curation, Software. **Zhao Yuan:** Data curation, Software. **Elena Vagnoni:** Writing – reviewing & editing. **Rachid Cherkaoui:** Supervision. **Mario Paolone:** Supervision, Project administration.

Declaration of competing interest

The authors declare that they have no known competing financial interests or personal relationships that could have appeared to influence the work reported in this paper.

Appendix. Forecasting tools

Once the optimization problem Eqs. (4a)–(4e) is defined, the challenge stands in the forecast of the prosumption and the frequency deviation, in particular their confidence intervals, denoting the maximum and minimum expected realizations, namely $L_n^{\uparrow}$, $L_n^{\downarrow}$ and $W_{f,k}^{\uparrow}$, $W_{f,k}^{\downarrow}$. As correctly appointed by [17], the local prosumption is characterized by a high volatility due to the reduced spatial smoothing effect of PV generation and the prominence of isolated stochastic events, such

as induction motors inrushes due to the insertion of pumps or elevators. For these reasons, the existing forecasting methodologies, developed by considering high levels of aggregation [46], are not suitable to predict low populated aggregates of prosumers. For the proposed application, the problem of identifying $L_n^{\uparrow}$ and $L_n^{\downarrow}$ is divided into two sub-problems: (i) load consumption forecast and (ii) PV production forecast. For the first one, a simple non-parametric forecasting strategy relying on the statistical properties of the time series is proposed. The PV production forecast is performed by taking advantage of solar radiation and meteorological data services providing a day-ahead prediction of the *Global Horizontal Irradiance* (GHI) together with its uncertainty. The GHI forecast, together with the information related to the PV installation (i.e. total capacity, location, tilt, azimuth) allows computing the *Global Normal Irradiance* (GNI) and obtaining an estimation of the total PV production, and the related uncertainties. The best and worst PV production scenarios are computed by transposing the GHI forecast data and applying a physical model of PV generation accounting for the air temperature [47]. For a given day-ahead forecast, the vector containing the best and worst production scenario for the PV, with a time resolution of 5 min are named as $\mathbf{PV}^{\uparrow}$ and $\mathbf{PV}^{\downarrow}$, respectively.

As previously mentioned, while the PV production forecast leverages GHI data, the load forecast only relies on statistical properties of recorded time-series. In particular, a set of historical observation $\mathcal{G}$ at the PCC point is considered. The historical load consumption $\boldsymbol{C}$ is computed for every time step n corresponding to a 5 min window and every day d, as:

$$\begin{aligned} &\mathcal{C}_{n,d} = \mathcal{G}_{n,d} - \mathcal{P}_{n,d} - \mathcal{PV}_{n,d} \\ &\forall n \in [1, N] \qquad \forall d \in [1, D] \end{aligned} \tag{29}$$

where $\mathcal{P}_n$ is the historical measure of the BESS power at time n and $\mathcal{PV}_n$ is the estimated PV production at the same time relying on the onsite measures of GHI, and D is the total number of recorded days. The process described by Eq. (29), also know as disaggregation, allows for the decoupling of the PV production and the load consumption $\mathcal{C}$, composed by 288 samples for each recorded day. The different consumption scenarios are generated by applying the following heuristic:

- The data-set $\boldsymbol{C}$ is divided into sub-sets $\Omega_{A,B,C,D1,D2}$ by selecting consumption data corresponding respectively to: (A) first working day of the week, i.e. Mondays or days after holidays; (B) central working days of the week, i.e. Tuesdays, Wednesdays and Thursdays; (C) last working day of the week, i.e. Friday or days before holidays; (D) holidays, i.e. Saturday (subcategory D1), Sundays and festivities (subcategory D2).
- For each sub-set, the statistical properties μ and σ are inferred as:

$$\begin{aligned} &\boldsymbol{\mu}_{\Omega} = \texttt{mean}(\boldsymbol{\Omega}) \qquad \boldsymbol{\sigma}_{\Omega} = \texttt{cov}(\boldsymbol{\Omega}) \\ &\forall \boldsymbol{\Omega} \in [\Omega_{A,B,C,D1,D2}] \end{aligned} \tag{30}$$

  where the function `mean` returns an array of 288 points, each of which represents a mean value for a particular 5-minutes window of the day and the function `cov` returns a 288×288 matrix corresponding to the covariance matrix of the observation.
- Both $\boldsymbol{\mu}_{\Omega}$ and $\boldsymbol{\sigma}_{\Omega}$ are computed by considering an exponential forgetting factor to prioritize the latest measurement with respect to the older one, as defined in [48].
- A given number S of possible scenarios is generated by considering the same multivariate normal distribution, with mean equal to μ and covariance equal to σ
- $\boldsymbol{C}^{\downarrow}$ and $\boldsymbol{C}^{\uparrow}$ are defined as the load scenarios characterized by the lowest and highest load profile, respectively.

Finally, the prosumption minimum end maximum expected realization are computed by combining $\boldsymbol{C}^{\downarrow}$ and $\boldsymbol{C}^{\uparrow}$ with $\boldsymbol{PV}^{\uparrow}$ and $\boldsymbol{PV}^{\downarrow}$ as follows:

$$L_n^{\uparrow} = C_n^{\uparrow} - PV_n^{\downarrow} \tag{31}$$

$$L_n^{\downarrow} = C_n^{\downarrow} - PV_n^{\uparrow} \tag{32}$$

$\forall n \in [1, N]$

Concerning the prediction of W_f, while [16] only relies on the statistical properties of the time series, this paper uses an auto regressive model, as supported by [49] which indicates the possibility to predict W_f to reduce the variance of the forecast in respect to the historical variance of the time series.

References

[1] CAISO, Frequency Response Phase 2, Tech. Rep., California ISO, 2016.
[2] ERCOT, Inertia:basic Concepts and Impact on the ERCOT Grid, Tech. Rep., Electricity Reliability Council of Texas, 2018.
[3] AEMO, Renewable Integration Study: stage 1 Report - Enabling Secure Operation of the NEM with Very High Penetrations of Renewable Energy, Tech. Rep., Australian Energy Market Operator, 2020.
[4] E. Rehman, M. Miller, J. Schmall, S. Huang, Dynamic Stability Assessment of High Penetration of Renewable Generation in the ERCOT Grid, Tech. Rep., ERCOT, Austin, Tx, 2018.
[5] AEMO, Maintaining Power System Security with High Penetrations of Wind and Solar Generation, 2019.
[6] B. Dunn, H. Kamath, J.-M. Tarascon, Electrical energy storage for the grid: A battery of choices, Science 334 (6058) (2011) 928–935.
[7] W.J. Cole, A. Frazier, Cost Projections for Utility-Scale Battery Storage, Tech. Rep., National Renewable Energy Lab.(NREL), Golden, CO (United States), 2019.
[8] P. Mercier, R. Cherkaoui, A. Oudalov, Optimizing a battery energy storage system for frequency control application in an isolated power system, IEEE Trans. Power Syst. 24 (3) (2009) 1469–1477.
[9] B. Lian, A. Sims, D. Yu, C. Wang, R.W. Dunn, Optimizing LiFePO4 battery energy storage systems for frequency response in the UK system, IEEE Trans. Sustain. Energy 8 (1) (2017) 385–394.
[10] K. Doenges, I. Egido, L. Sigrist, E. Lobato Miguélez, L. Rouco, Improving AGC performance in power systems with regulation response accuracy margins using battery energy storage system (BESS), IEEE Trans. Power Syst. 35 (4) (2020) 2816–2825.
[11] A. Giannitrapani, S. Paoletti, A. Vicino, D. Zarrilli, Optimal allocation of energy storage systems for voltage control in LV distribution networks, IEEE Trans. Smart Grid 8 (6) (2017) 2859–2870.
[12] T. Zhao, A. Parisio, J.V. Milanović, Distributed control of battery energy storage systems in distribution networks for voltage regulation at transmission–distribution network interconnection points, Control Eng. Pract. 119 (2022) 104988.
[13] R. Gupta, F. Sossan, M. Paolone, Grid-aware distributed model predictive control of heterogeneous resources in a distribution network: Theory and experimental validation, IEEE Trans. Energy Convers. 36 (2) (2020) 1392–1402.
[14] AEMO, Initial operation of the Hornsdale Power Reserve Battery Energy Storage System, Technical Report, Apr, 2018.
[15] O. Mégel, J.L. Mathieu, G. Andersson, Scheduling distributed energy storage units to provide multiple services under forecast error, Int. J. Electr. Power Energy Syst. 72 (2015) 48–57, The Special Issue for 18th PSCC.
[16] E. Namor, et al., Control of battery storage systems for the simultaneous provision of multiple services, IEEE Trans. Smart Grid 10 (3) (2019) 10.
[17] F. Sossan, E. Namor, R. Cherkaoui, M. Paolone, Achieving the dispatchability of distribution feeders through prosumers data driven forecasting and model predictive control of electrochemical storage, IEEE Trans. Sustain. Energy (2016).
[18] A. Zecchino, Z. Yuan, F. Sossan, R. Cherkaoui, M. Paolone, Optimal provision of concurrent primary frequency and local voltage control from a BESS considering variable capability curves: Modelling and experimental assessment, Electr. Power Syst. Res. 190 (2021) 106643.
[19] Y. Zuo, Z. Yuan, F. Sossan, A. Zecchino, R. Cherkaoui, M. Paolone, Performance assessment of grid-forming and grid-following converter-interfaced battery energy storage systems on frequency regulation in low-inertia power grids, Sustain. Energy Grids Netw. (2021).
[20] A. Reza Reisi, M. Hassan Moradi, S. Jamasb, Classification and comparison of maximum power point tracking techniques for photovoltaic system: A review, Renew. Sustain. Energy Rev. 19 (2013) 433–443.
[21] J.A. Baroudi, V. Dinavahi, A.M. Knight, A review of power converter topologies for wind generators, Renew. Energy 32 (14) (2007) 2369–2385.
[22] J. Beerten, O. Gomis-Bellmunt, X. Guillaud, J. Rimez, A. van der Meer, D. Van Hertem, Modeling and control of HVDC grids: A key challenge for the future power system, in: 2014 Power Systems Computation Conference, 2014, pp. 1–21.
[23] Y. Lin, J.H. Eto, B.B. Johnson, J.D. Flicker, R.H. Lasseter, H.N. Villegas Pico, G.-S. Seo, B.J. Pierre, A. Ellis, Research Roadmap on Grid-Forming Inverters, Tech. Rep., National Renewable Energy Lab.(NREL), Golden, CO (United States), 2020.
[24] J. Matevosyan, B. Badrzadeh, T. Prevost, E. Quitmann, D. Ramasubramanian, H. Urdal, S. Achilles, J. MacDowell, S.H. Huang, V. Vital, J. O'Sullivan, R. Quint, Grid-forming inverters: Are they the key for high renewable penetration? IEEE Power Energy Mag. 17 (6) (2019) 89–98.

[25] G. Denis, T. Prevost, P. Panciatici, X. Kestelyn, F. Colas, X. Guillaud, Review on potential strategies for transmission grid operations based on power electronics interfaced voltage sources, in: 2015 IEEE Power Energy Society General Meeting, 2015, pp. 1–5.
[26] Y. Zuo, M. Paolone, F. Sossan, Effect of voltage source converters with electrochemical storage systems on dynamics of reduced-inertia bulk power grids, Electr. Power Syst. Res. 189 (2020) 106766.
[27] J. Liu, Y. Miura, T. Ise, Comparison of dynamic characteristics between virtual synchronous generator and droop control in inverter-based distributed generators, IEEE Trans. Power Electron. 31 (5) (2016) 3600–3611.
[28] T. Qoria, E. Rokrok, A. Bruyere, B. Francois, X. Guillaud, A PLL-free grid-forming control with decoupled functionalities for high-power transmission system applications, IEEE Access 8 (2020) 197363–197378.
[29] R. Rosso, S. Engelken, M. Liserre, Robust stability analysis of synchronverters operating in parallel, IEEE Trans. Power Electron. 34 (11) (2019) 11309–11319.
[30] S. Lu, P.V. Etingov, D. Meng, X. Guo, C. Jin, N.A. Samaan, NV Energy Large-Scale Photovoltaic Integration Study: intra-Hour Dispatch and AGC Simulation, Tech. Rep., Pacific Northwest National Lab.(PNNL), Richland, WA (United States), 2013.
[31] C. Hodel, Overview of ancillary services, 2019, URL https://www.swissgrid.ch/dam/swissgrid/customers/topics/ancillary-services/as-documents/AS-concept-V1-1-en.pdf.
[32] S. Ltd, Balancing roadmap Switzerland, 2018, URL https://www.swissgrid.ch/dam/swissgrid/about-us/newsroom/publications/balancing-roadmap-ch-en.pdf.
[33] W. Sattinger, Test zur sekundärregelfähigkeit, 2020, URL https://www.swissgrid.ch/dam/swissgrid/customers/topics/ancillary-services/prequalification/3/F20200529-test-for-primary-control-capability-de.pdf.
[34] S. Margelou, Präqualifikationsunterlagen primärregelung, 2020, URL https://www.swissgrid.ch/dam/swissgrid/customers/topics/ancillary-services/prequalification/3/F20200529-prequalification-documents-primary-control-de.pdf.
[35] T. Ott, Requirements for schedule data, 2020, URL https://www.swissgrid.ch/dam/swissgrid/customers/topics/ancillary-services/prequalification/1/D200630-requirements-schedule-and-electronic-data-V8R0_en.pdf.
[36] A. Kaushal, D.V. Hertem, An overview of ancillary services and HVDC systems in European context, Energies 12 (18) (2019) 3481.
[37] Regelleistung website, Internet platform for the allocation of control power, 2021, URL https://www.regelleistung.net. (Accessed 04 October 2021).
[38] Commission regulation (EU) 2016/ 631 - of 14 April 2016 - establishing a network code on requirements for grid connection of generators, Off. J. Eur. Union (2016) 68.
[39] B. Dunn, H. Kamath, J.-M. Tarascon, Electrical energy storage for the grid: A battery of choices, Science 334 (6058) (2011) 928–935.
[40] W.J. Cole, A. Frazier, Cost Projections for Utility-Scale Battery Storage, Tech. Rep. NREL/TP-6A20-73222, 1529218, National Renewable Energy Laboratory, 2019.
[41] E. Scolari, L. Reyes-Chamorro, F. Sossan, M. Paolone, A comprehensive assessment of the short-term uncertainty of grid-connected PV systems, IEEE Trans. Sustain. Energy 9 (3) (2018) 1458–1467.
[42] M. Bahramipanah, D. Torregrossa, R. Cherkaoui, M. Paolone, Enhanced electrical model of Lithium-based batteries accounting the charge redistribution effect, in: 2014 Power Systems Computation Conference, 2014, pp. 1–8.
[43] M. Pignati, et al., Real-time state estimation of the EPFL-campus medium-voltage grid by using PMUs, in: 2015 IEEE Power & Energy Society Innovative Smart Grid Technologies Conference, ISGT, IEEE, Washington, DC, USA, 2015, pp. 1–5.
[44] L. Zanni, A. Derviškadić, M. Pignati, C. Xu, P. Romano, R. Cherkaoui, A. Abur, M. Paolone, PMU-based linear state estimation of Lausanne subtransmission network: Experimental validation, in: 21st PSCC, 2020.
[45] A. Zecchino, F. Gerini, Y. Zuo, R. Cherkaoui, M. Paolone, E. Vagnoni, Local effects of grid-forming converters providing frequency regulation to bulk power grids, in: 2021 IEEE PES Innovative Smart Grid Technologies-Asia (ISGT Asia), IEEE, 2021, pp. 1–5.
[46] B.-J. Chen, M.-W. Chang, C.-J. Lin, Load forecasting using support vector machines: A study on EUNITE competition 2001, IEEE Trans. Power Syst. 19 (4) (2004) 1821–1830.
[47] F. Sossan, et al., Solar irradiance estimations for modeling the variability of photovoltaic generation and assessing violations of grid constraints: A comparison between satellite and pyranometers measurements with load flow simulations, J. Renew. Sustain. Energy 11 (5) (2019) 056103.
[48] F. Pozzi, T. Di Matteo, T. Aste, Exponential smoothing weighted correlations, Eur. Phys. J. B 85 (6) (2012) 175.
[49] G. Piero Schiapparelli, S. Massucco, E. Namor, F. Sossan, R. Cherkaoui, M. Paolone, Quantification of primary frequency control provision from battery energy storage systems connected to active distribution networks, in: 2018 Power Systems Computation Conference, PSCC, IEEE, Dublin, 2018, pp. 1–7.